energy&fuels

pubs.acs.org/EF
Article

Inverse Consequences of the SnO_2 Protection Layers on Pt/C Catalysts in Proton-Exchange Membrane Fuel Cells

Published as part of Energy & Fuels virtual special issue "2024 Energy and Fuels Rising Stars".

Young-Woon Byeon,[‖] Shirin Mehrazi,[‖] Björn M. Stühmeier, Venkata Sai Avvaru, Dong-Min Kim, Brett A. Helms, Lei Cheng,* and Haegyeom Kim*

Cite This: *Energy Fuels* 2024, 38, 14655−14662

Read Online

ACCESS | Metrics & More | Article Recommendations | Supporting Information

ABSTRACT: Proton-exchange membrane fuel cells (PEMFCs) are promising energy-conversion systems, offering an appealing blend of high energy efficiency and low environmental impact. However, carbon corrosion of PEMFCs is known to significantly degrade their performance, remaining a critical challenge to overcome. In this study, we applied a Nb-doped SnO_2 (Nb−SnO_2) nanoparticle coating on Pt/C catalysts as a protective layer, with the Sn/C ratio in the precursors varying from 0.25:1 to 2.0:1. Contradictory behaviors of the coated Pt/C catalysts were observed at different Sn/C ratios. The Sn/C = 1.0 sample exhibited improved electrochemically active surface area retention after 500 cycles of accelerated stress testing (AST) but with more significant polarization and resistance increase observed in the polarization curves. In addition, agglomeration of Nb−SnO_2 particles was observed at a higher Sn/C ratio in the AST of a membrane electrode assembly, with less shrinkage of the total thickness of the Nb−SnO_2-coated Pt/C electrode. We speculate that formation of Nb−SnO_2 agglomerates occurs once the protective layer is broken down or the unprotected carbon surface is corroded and that these Nb−SnO_2 agglomerates increase the tortuosity of the electron pathways and significantly increase the cell polarization.

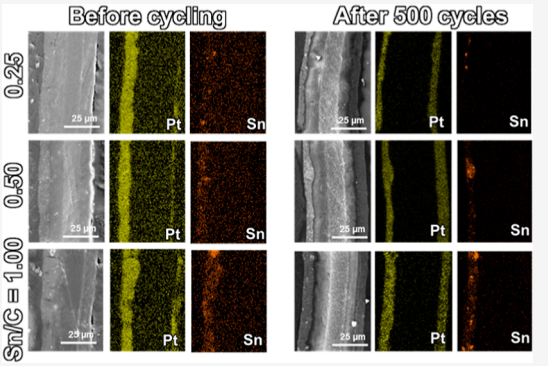

1. INTRODUCTION

Electrification is at the forefront of revolutionizing modern society toward more sustainable and efficient solutions for energy generation and consumption. As the push for achieving a renewable society intensifies, the quest for reliable, accessible, high-performance power sources has become of paramount importance. Proton-exchange membrane fuel cells (PEMFCs) have attracted significant attention, offering an appealing blend of high energy efficiency and low environmental impact, which is especially critical for the transportation sector.[1−3] The current demand for modern transportation can be fulfilled by the sustainable energy generation provided by PEMFCs, providing benefits compared with the limited energy storage of secondary batteries or the intermittent energy generation offered by photovoltaics.[4,5] This ensures a consistent and on-demand energy supply crucial for meeting the demands of modern transportation.[4]

Despite their high energy efficiency, the durability of PEMFCs remains a significant challenge, particularly for transportation applications, where the operating conditions can accelerate performance degradation.[6] One of the most detrimental modes of degradation in fuel cells is carbon corrosion.[7−9] In PEMFCs, the catalytic layer consists of a catalyst [i.e., platinum (Pt)], catalyst support [i.e., carbon (C)], and Nafion polymer and plays a key role in the electrochemical conversion of hydrogen and oxygen into electricity. Strong contact between the Pt and carbon support is necessary to provide the electron-transport pathways required for the electrochemical reactions.[6,8] However, carbon is not thermodynamically stable under the operating conditions of PEMFCs, and the electrochemical degradation of the carbon support is further accelerated at elevated potential and temperatures. Upon the degradation of carbon, the Pt catalysts become detached from the support and form agglomerates, leading to a significant loss of an electrochemically active Pt surface area.[9−11]

Many researchers have devoted significant efforts to address the degradation of carbonaceous supports to enhance the durability of PEMFCs.[12−14] Xue et al. and Qiao et al. demonstrated the improved stability of highly graphitized carbon under PEMFC operating conditions compared with

Received: May 12, 2024
Revised: June 28, 2024
Accepted: July 1, 2024
Published: July 11, 2024

https://doi.org/10.1021/acs.energyfuels.4c02232
Energy Fuels 2024, 38, 14655−14662

that of amorphous carbon or carbon with a functionalized surface,[13,14] and Wu et al. proposed graphene as a catalyst support with improved durability.[12] Noncarbonaceous materials have also been suggested as catalyst-supporting materials. For example, Wei et al. developed a TiN−TiO_2 composite as a Pt-catalyst support through alkali treatment and highlighted its synergistic benefits.[15] TiN offers high electrical conductivity while TiO_2 provides good corrosion resistance. Similarly, we previously introduced $Mg_{1-x}Ti_{2+x}O_{5-y}$ ternary compounds, aiming to simultaneously achieve high conductivity and strong acidic stability.[16] A high synthesis temperature of 1500 °C was selected to further improve the conductivity by reducing the oxidation state of Ti in the structure. However, this approach presents challenges in achieving a large surface area comparable to that of commercial carbonaceous supports because of the high-temperature synthesis process required. Lee et al. proposed Ti^{3+}-enriched N,C-codoped mixed-phase TiO_2 nanoparticles as a stable catalyst support; they reduced the oxidation state of Ti and corresponding band gap to increase the electrical conductivity.[17] Oxygen-deficient TiO_2[18] and antimony- and niobium-doped SnO_2 particles[19−21] have also been investigated as potential catalyst supports for PEMFCs.

In the current study, instead of using Nb-doped SnO_2 (Nb−SnO_2) as a Pt catalyst support,[19−21] we applied a Nb-doped SnO_2 nanoparticle coating on Pt/C catalysts to enhance the corrosion resistance of the carbon without compromising the functionality of the Pt catalysts. In fact, SnO_2 and doped SnO_2 have been studied as catalyst support materials to replace carbon support in PEMFC because of their good durability in oxidative conditions.[22−25] However, SnO_2 is a poor electron conductor and doped SnO_2 exhibits much lower electronic conductivity than carbon despite improved electronic conductivity by doping.[24−26] Herein, we applied the Nb−SnO_2 coating as a protection for the carbon support in Pt/C to combine the good stability of Nb−SnO_2 coating layer and the high electronic conductivity of a carbon framework. We expected that the residual functional groups on carbon, which are typically negatively charged, would attract Sn^{4+} and form a preferred anchoring to bind SnO_2 nanoparticles. The main purpose of the Nb−SnO_2 coating is to protect the electrode from abusive carbon corrosion. The Nb doping was intended to increase the electronic conductivity of the SnO_2 coating layers because we expect that a more electronically conductive coating layer (Nb−SnO_2 vs SnO_2) would be beneficial.[19] The Nb−SnO_2 coating layer resulted in improved retention of the electrochemically active surface area (ECSA) of the Pt/C catalysts after accelerated stress testing (AST) of a membrane electrode assembly (MEA). However, unexpectedly, the cell polarization increased significantly when thicker Nb−SnO_2 coating layers were applied. These contradictory results can be explained by the formation of Nb−SnO_2 particle agglomerates after long-term cycling, which may block the electron pathways due to their relatively lower electronic conductivity compared to carbon.

2. EXPERIMENTAL SECTION

2.1. Material Preparation. The appropriate amounts of $SnCl_4 \cdot 5H_2O$ (98%, Sigma-Aldrich) and $NbCl_5$ (99.9%, anhydrous, Sigma-Aldrich) were dissolved in an isopropyl alcohol (IPA) solution using ultrasonication, maintaining a Sn/Nb weight ratio of 96:4. Subsequently, this solution was combined with Pt/C particles dispersed in water (3.0 mg mL^{-1}), achieving initial salt precursor-to-carbon weight ratios of 0.25:1, 0.50:1, 1.0:1, and 2.0:1. The mixture was then stirred at 350 rpm for 3 h in a 50 °C oil bath, followed by the dropwise addition of 60 mL of 0.15 M urea aqueous solution. Stirring continued for an additional 3 h. Afterward, the resultant product was thoroughly washed with Milli-Q water until a neutral pH was reached. Finally, the material was dried in an oven at 70 °C.

2.2. Characterization. X-ray diffraction (XRD) analysis was conducted using a Rigaku Miniflex 600 equipped with a Cu-Kα radiation source (λ = 1.5406 Å). The elemental compositions of Nb, Sn, and Pt in each composite sample were determined using inductively coupled plasma optical emission spectrometry (ICP-OES; Agilent 5110). The surface morphology and microstructure of the Nb−SnO_2 composite powders were examined using scanning electron microscopy (SEM; PHENOM PW-100-017) with an acceleration voltage of 15 kV. Energy-dispersive X-ray spectroscopy (EDS) elemental mappings were also obtained using transmission electron microscopy (TEM; FEI TitanX 60-300) at an acceleration voltage of 300 kV. To prevent e-beam-induced sample damage, each elemental mapping was collected for less than 4 min. Specific X-ray edges (C-Kα, O-Kα, Sn-Lα, Pt-Lα, and Nb-Kα) were selected to avoid energy overlaps between certain elements in the samples. Thermogravimetric analysis (TGA) was performed with a TGA5500 (TA Instruments) using a Pt pan. The measurements were conducted at a heating rate of 5 °C min^{-1} from 25 to 600 °C under an O_2 gas flow environment. To remove absorbed moisture on the sample surface, all samples were dried in a desiccator overnight before each measurement.

MEA cross-sectional SEM and EDS mapping were performed using a JSM-7200F field-emission scanning electron microscope equipped with an Oxford Instruments/$XMAX^N$ EDS detector. The EDS data was collected using AZTEC.EDS software. The epoxy mounting/cutting method was used to prepare cross sections for SEM analysis. An area of approximately 0.5 cm × 0.5 cm at the active region of the MEA was first cut and was then sandwiched between gas diffusion layers (GDLs) and held flat with stainless-steel plates. The entire assembly was mounted in epoxy and then sectioned to expose the cross section. The cross section was further polished using multiple polishing papers with the finish progressively increasing from 320 to 1200 grit.

2.3. Electrochemical Testing. *2.3.1. MEA Fabrication.* The synthesized Nb−SnO_2-coated catalyst powders were mixed with a solution of ionomer (D2020), deionized water, and IPA. The ionomer to carbon-support (I/C) ratio (mass ratio) and the solvent to carbon-support ratio (mass ratio) were fixed at 0.55 and 0.038, respectively. The ratio of deionized water to IPA in our experiment is fixed to be 1 (mass ratio). Centrifugal planetary mixing (Thinky mixer) with 5 mm zirconia beads was used to prepare the catalyst ink. The ink was then coated on a virgin PTFE substrate using the Mayer rod method, and the coated film was subsequently dried in air. The wet film thickness was adjusted to achieve 0.2 mg/cm^2 of catalyst loading for all Nb−SnO_2-coated Pt compounds. Anode catalyst ink was prepared using the same mixing method as the cathode catalyst ink using 20% Pt on carbon XC-72R (Fuelcell store), Nafion D2020, and a mixture of IPA and DI water as the solvent. The I/C ratio of the anode catalyst ink was 0.85, and the loading of the coated anode catalyst layer was 0.1 mg/cm^2. Catalyst-coated decals (anode and cathode) were transferred to a Nafion-XL (Ion Power) membrane via hot pressing at 135 °C to prepare each MEA.

2.3.2. Cell Assembly. MEAs with an active area of 4 cm^2 were assembled with the anode and cathode GDLs (anode/cathode AvCarb GDS3250 and MB30, respectively; GDS3250:PTFE-treated carbon fiber paper coated with a microporous layer, thickness = 225 μm; MB30:PTFE-treated carbon fiber paper coated with a microporous layer, thickness = 205 μm) in Baltic fuel-cell hardware with straight parallel flow fields on both anode and cathode side. The cell hardware was installed on a fuel-cell test stand (Evaluator C50-LT, HORIBA FuelCon) and was compressed to 150 kPa.

2.3.3. AST of the MEA and Electrochemical Measurements. Before electrochemical tests, the assembled MEAs were broken in by a voltage cycling protocol between OCV, 0.6 V, and 0.3 V in the H_2/

https://doi.org/10.1021/acs.energyfuels.4c02232
Energy Fuels 2024, 38, 14655−14662

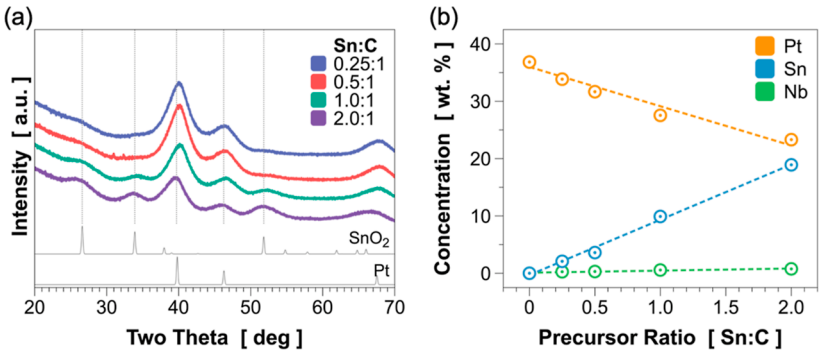

Figure 1. (a) XRD patterns and (b) atomic concentration profiles of Nb−SnO_2-coated Pt/C compounds with different Sn/C precursor ratios.

air (anode/cathode) environment at 80 °C and 100% relative humidity (RH) for 2 h, the flow rates were 0.4 normal liter per minute (NLPM) H_2 (anode) and 1.5 NLPM air (cathode), respectively. ASTs were performed using a Gamry Instruments reference 3000 potentiostat and the polarization curves were performed using a load-bank of the HORIBA FuelCon fuel cell test stand with a maximum current load of 100 A. The ASTs were performed using a triangular-wave potential scanning between 1 and 1.5 V with 1 s ramp duration (i.e., 0.5 V s^{-1} scan rate) at 80 °C and 100% RH and a constant flow rate of 0.5 NLPM H_2 (anode) and 1.0 NLPM air (cathode). ASTs were tested up to 500 cycles. Electrochemical characterization was done at the beginning of life (BOL, 0 cycles of AST), 250 cycles of AST, and 500 cycles of AST. CV measurements were carried out in a potential window of 0.075 and 0.9 V with a scan rate of 50 mV s^{-1} in H_2/N_2 environment (anode/cathode) with a flow rate of 0.2/0.8 NLPM, respectively. LSV measurements were carried out between 0.05 and 0.5 V with a scan rate of 1 mV s^{-1}. Polarization curves were measured in H_2/air (anode/cathode) environment at 80 °C and 100% RH, starting with current steps stepping from high to low current densities. During the polarization curve measurement, constant flow rates of 1.3 NLPM H_2 and 4 NLPM air were maintained. EIS was performed between the frequencies of 50,000 and 100 Hz. LSV measurements were performed at 100% RH. EIS measurements were done during each potential hold to extract the various resistances of the cell at that specific current density.

3. RESULTS

3.1. Structure and Morphology Analysis of Nb−SnO_2-Coated Pt/C Compounds. We synthesized Nb-doped SnO_2 (Nb−SnO_2)-coated Pt/C catalyst particles using a solution-based route to protect the carbon surface from corroding and to improve the durability of the PEMFCs. Figure 1a presents XRD patterns of the Nb−SnO_2-coated Pt/C samples with varied Sn/C weight ratios used in the precursors during the synthesis process. We synthesized four samples with Sn/C weight ratios ranging from 0.25:1 to 2.0:1. As the Sn/C ratio increases, the diffraction peaks of SnO_2 become more obvious while the peak intensity of Pt decreases. These changes indicate that the higher Sn precursor ratio in the precursors leads to the formation of a thicker Nb−SnO_2 protecting layer. Some minor impurity peaks appeared at ∼31 and ∼33° for the sample with Sn/C = 0.5:1; however, these peaks could not be matched with any known phases due to their low intensity. Figure 1b presents the compositions obtained from ICP analysis. The composition of a Pt/C reference consisted of 37 wt % Pt. With increasing Sn/C ratio, the concentrations of Sn and Nb linearly increased, whereas that of Pt decreased. The concentrations of Sn and Nb increased from 2.1 wt % (Sn) and 0.26 wt % (Nb) for a Sn/C precursor ratio of 0.25:1 to 19 wt % (Sn) and 0.76 wt % (Nb) for a Sn/C precursor ratio of 2.0:1, whereas that of Pt decreased from 34 wt % to 23 wt %. TGA was also conducted to confirm the carbon concentration changes upon changing the Sn/C ratio (Figure S1 in the Supporting Information). The carbon content decreased with an increasing Sn/C ratio in the precursors. The carbon content in the Pt/C reference was 60 wt % and this value further decreased from 53 wt % for Sn/C = 0.25:1 to 34 wt % for Sn/C = 2.0:1.

Figure 2 presents SEM images and corresponding EDS mapping images of Nb−SnO_2-coated Pt/C samples prepared

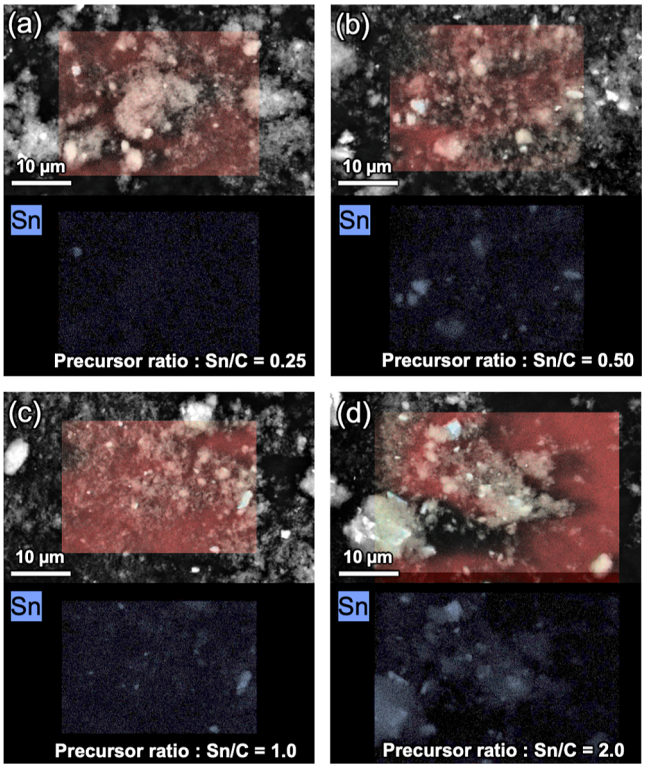

Figure 2. SEM images and Sn-L elemental mappings of Nb−SnO_2-coated Pt/C samples at various Sn/C precursor ratios: (a) 0.25, (b) 0.50, (c) 1.0, and (d) 2.0.

using various Sn/C precursor ratios before MEA fabrication. No secondary elements other than Nb, Sn, C, and O were detected in the four samples in the EDS spectrum (Figure S2 in the Supporting Information). For the Sn/C precursor ratio of 0.25:1, Sn was uniformly distributed within the sample. However, secondary particles with higher Sn concentrations started to form when the Sn/C precursor ratio increased. When the ratio reached 2.0:1, large Sn-concentrated particles

https://doi.org/10.1021/acs.energyfuels.4c02232
Energy Fuels 2024, 38, 14655−14662

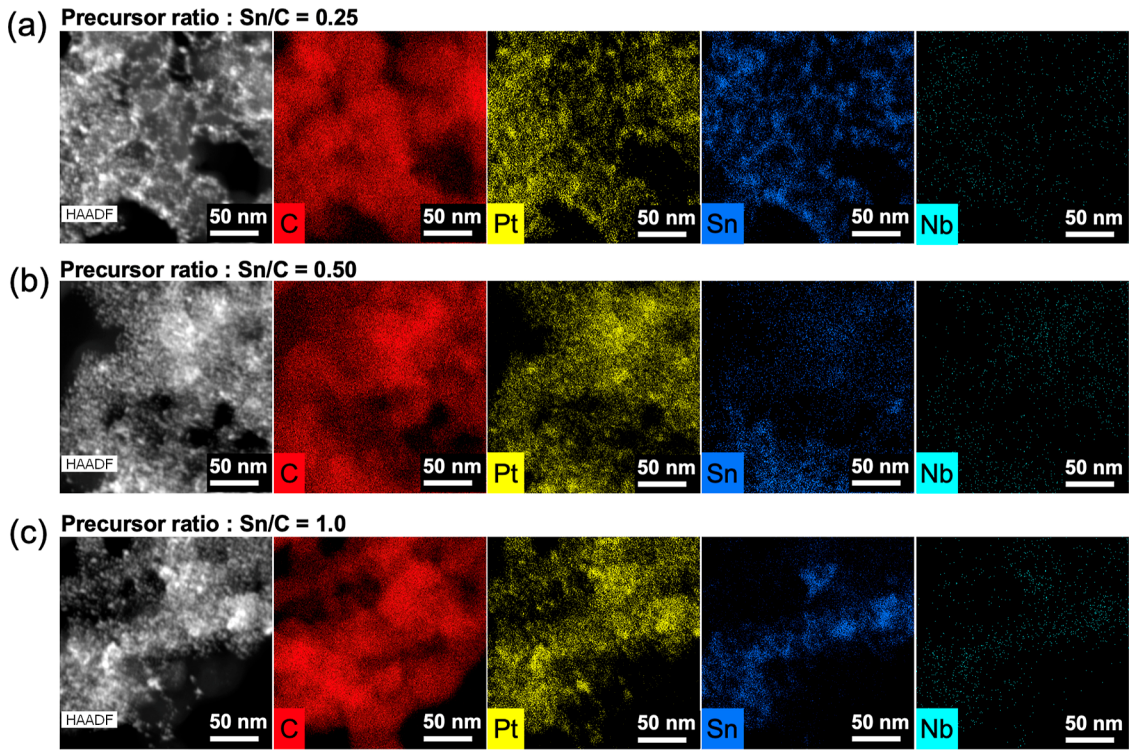

Figure 3. STEM-HAADF images and corresponding elemental mappings of C, Pt, Sn, and Nb at various Sn/C precursor ratios: (a) 0.25, (b) 0.50, and (c) 1.0.

Table 1. ECSA Retention across Various Cycling Stages in AST Using MEA

Sn/C ratio in precursors	Pt loading (mg/cm^2)	ECSA before cycling (m^2/mg_{Pt})	ECSA after 250 cycles (m^2/mg_{Pt})	ECSA after 500 cycles (m^2/mg_{Pt})	ECSA retention after 500 cycles (%)
0.0 (Pt/C only)	0.20	46	22	16	34.7
0.25	0.21	37	19	10	27.0
0.5	0.25	38	32	18	47.4
1.0	0.24	38	30	17	44.7

(>10 μm) appeared in the SEM and EDS mapping images (Figure 2d). As we expect that such a large secondary Sn-concentrated particle could not serve as a protecting layer against carbon corrosion in PEMFCs, we focus on the structural analysis and electrochemical performance of the samples with Sn/C ratios of 1.0:1, 0.50:1, and 0.25:1 hereafter.

To better understand and evaluate the distributions of Pt, C, Sn, and Nb in the Nb−SnO_2-coated Pt/C samples, we performed STEM-EDS elemental mapping analysis, as shown in Figure 3 (see Figure S3 in Supporting Information for the EDS spectra for each mapping). As expected, we confirmed that the Pt nanoparticles were uniformly decorated on the carbon surface in all three samples. Nb−SnO_2 protecting layers were confirmed to be uniformly distributed throughout the samples. For the Sn/C precursor ratio of 1.0:1, relatively large Sn-concentrated (Nb−SnO_2) particles were observed in the STEM-EDS mapping (Figure 3c). The Nb concentration used in our samples is less than 1 wt % (Figure 1b). Therefore, the EDS signal for Nb is relatively low, which makes it difficult to capture a clear EDS mapping of Nb in Figure 3.

3.2. Electrochemical Performance. We evaluated the ECSA retention of MEA cells containing Nb−SnO_2-coated Pt/C samples with varied Sn/C ratios before and after cycling (Table 1). Based on the ICP analysis results of the Pt content in the Nb−SnO_2-coated Pt/C samples, we adjusted the wet film thickness to have similar Pt loading in the electrode among the samples. We found that the ECSAs per mass of the Pt catalyst before cycling decrease slightly after the Nb−SnO_2 coating but the ECSAs among the three samples with varied Sn/C ratios were similar, indicating that the Nb−SnO_2 coating layer does not cover the electrochemically active Pt surfaces substantially. Nb−SnO_2 would preferably be grown on the carbon surface, which exhibits negatively charged surfaces that attract Sn^{4+} during the synthesis process. Nevertheless, we expect that some Pt sites covered by Nb−SnO_2 would not act as catalysts.

AST was performed following the U.S. Department of Energy standard protocol to accelerate catalyst degradation.[27] After 250 and 500 cycles, the ECSA values noticeably decreased. The sample with a Sn/C precursor ratio of 0.25:1 showed a significant ECSA decrease from an initial 37 m^2/mg_{Pt} to 19 and 10 m^2/mg_{Pt} after 250 and 500 cycles, respectively. The ECSA retention after 500 cycles was only 27%. In contrast, the samples with higher Sn/C precursor ratios exhibited enhanced ECSA retention of >44% after 500 cycles. A slightly higher ECSA retention of 47.4% was achieved in the sample with a Sn/C precursor ratio of 0.50:1. In contrast, the commercial Pt/C catalyst exhibits ~35% of ECSA retention after 500 cycles.

https://doi.org/10.1021/acs.energyfuels.4c02232
Energy Fuels 2024, 38, 14655−14662

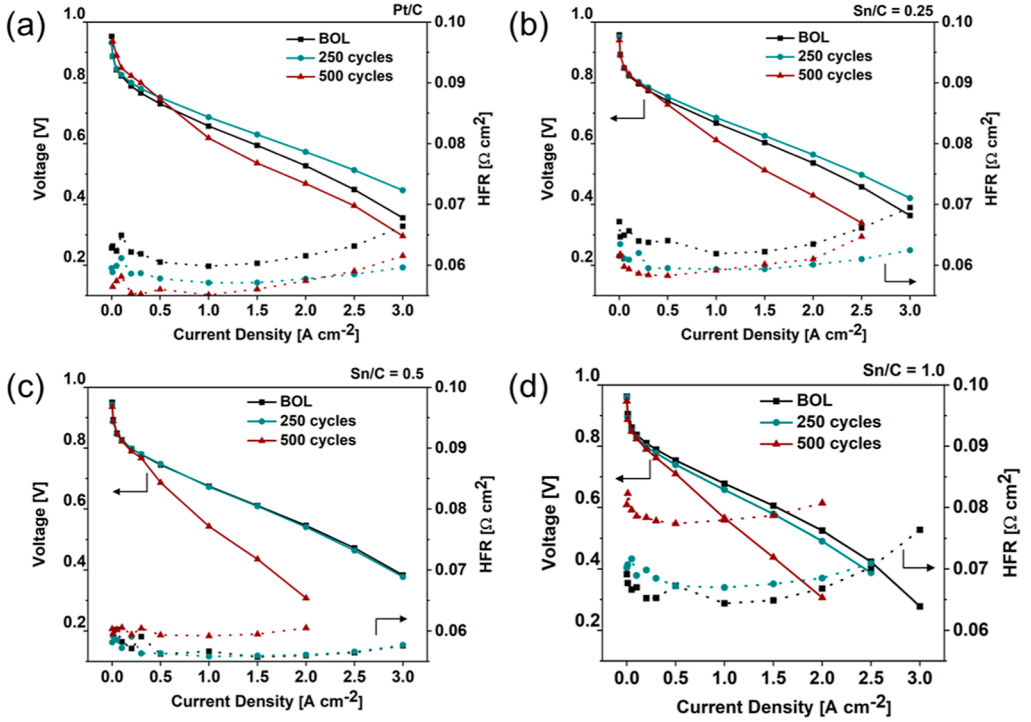

Figure 4. Voltage vs current density curves for (a) Pt/C catalyst and Nb−SnO_2 coated Pt/C catalysts with different Sn/C ratios of (b) 0.25, (c) 0.50, and (d) 1.0, illustrating the electrochemical performance variation with the Sn content in the precursor.

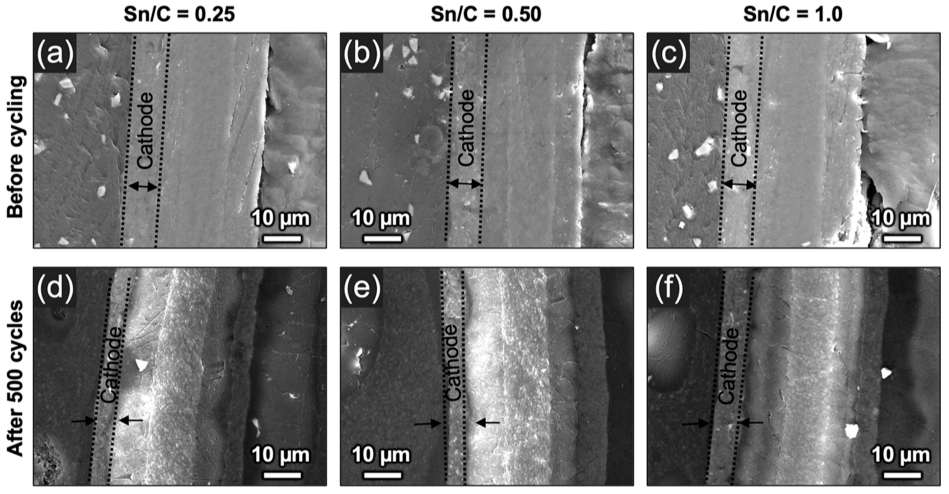

Figure 5. SEM images showing cross-sectional views of membranes: (a−c) at BOL and (d−f) after 500 cycles. Cathodes with a lower Sn/C ratio exhibited more significant shrinkage of the thickness postcycling.

The fuel-cell performance and durability of catalyst-coated membranes prepared using different Sn/C ratios of catalyst materials were evaluated by examining polarization curves at BOL and 250 and 500 cycles of AST, as shown in Figure 4. At BOL, Sn/C = 0.25 and Sn/C = 0.5 showed similarly good polarization curve performance and initial high frequency resistance (HFR). However, the initial performance of Sn/C = 1.0 was worse than that for the lower Sn/C ratios and Pt/C catalyst reference. Nonetheless, because this difference is not substantial, we speculate that there are no significant electrical conductivity changes in the MEA as a function of the Sn/C ratios. Upon carbon-corrosion AST cycling at 1.0−1.5 V for 250 cycles, none of the samples exhibited significant performance degradation. For the lower Sn/C ratio, even some performance improvements were observed, mostly in the transport region. This result was attributed to the improved O_2 transport due to pore opening in the cathode electrode resulting from carbon corrosion.[28] After 500 cycles, upon further carbon corrosion, the polarization curve performance of the samples with the higher Sn/C ratios of 0.5 and 1.0 degraded more compared with the limited total performance degradation of the sample with the Sn/C ratio of 0.25 and even compared with Pt/C catalyst reference. A similar trend of HFR increase was also observed for the cell assembly for higher Sn/C ratios. For Sn/C = 1.0, the HFR increased from approximately 0.06 to 0.08 Ω cm^2, whereas the HFR largely remained the same (in the range from approximately 0.06 to 0.065 Ω cm^2) for the lower Sn/C ratio samples. The trend of polarization curve performance loss is opposite to that of the ECSA results (in Table 1), where better ECSA retention was

https://doi.org/10.1021/acs.energyfuels.4c02232
Energy Fuels 2024, 38, 14655−14662

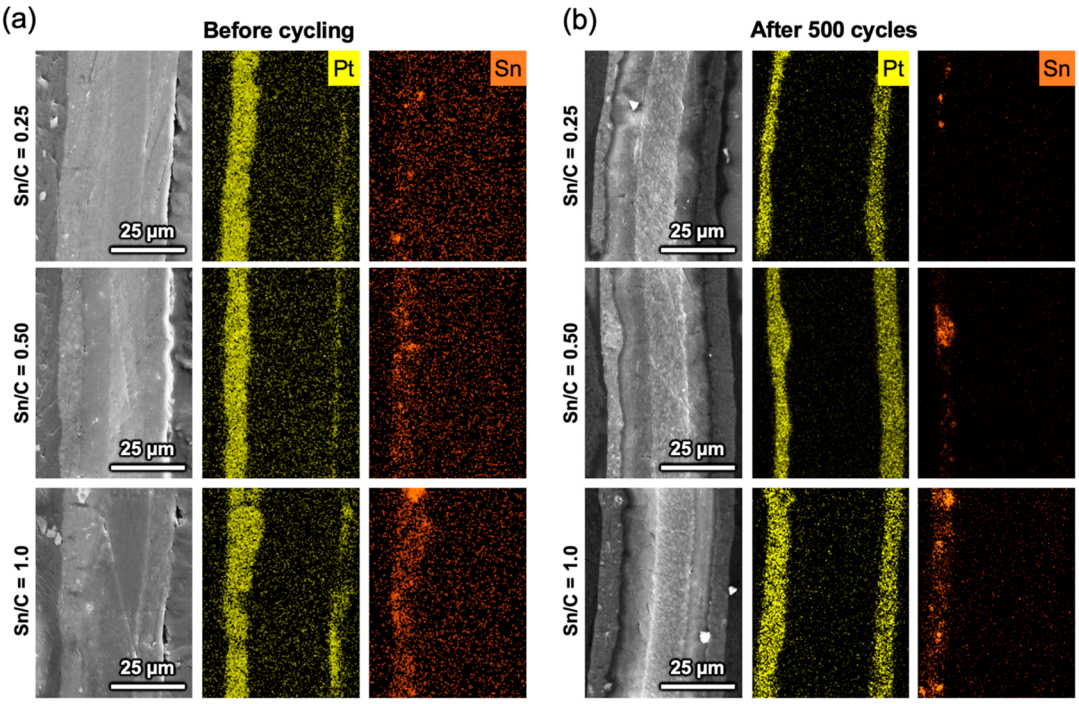

Figure 6. SEM-EDS elemental mappings of cross sections of various MEA cells: (a) at BOL and (b) after 500 cycles.

observed for the higher Sn/C ratio samples. To elucidate this performance discrepancy, a systematic post-mortem analysis was performed, as discussed in the following section.

3.3. Morphological Changes of Nb−SnO_2-Coated Pt/C Electrodes after PEMFC Tests. In our electrochemical testing, we found that the higher concentration of the Nb−SnO_2 coating layer resulted in improved retention of ECSA but faster performance degradation such as accelerated polarization and resistance increases after 500 cycles, which is indeed contradictory. In general, the decrease of ECSA after AST cycling indicates carbon corrosion and agglomeration of Pt catalysts, leading to an increase in polarization and resistance.[7,29] To better understand these inverse consequences (improved ECSA retention but increased polarization) by Nb−SnO_2 coating, we examined the morphological changes of the Nb−SnO_2-coated Pt/C electrodes after the stability test. SEM analysis of the Nb−SnO_2-coated Pt/C electrodes was conducted before the MEA test and after 500 cycles. Figure 5a−c displays the cross-sectioned SEM images of the Nb−SnO_2-coated Pt/C electrodes at varied precursor ratios of Sn/C. The thickness of the Nb−SnO_2-coated Pt/C electrode was ∼10 μm. Figure 5d−f presents cross-sectioned SEM images of the Nb−SnO_2-coated Pt/C electrodes after 500 cycles. The thickness of the electrode decreased significantly, by approximately 50%, at the low Sn/C precursor ratio (Sn/C = 0.25). In contrast, the electrodes with higher Sn/C precursor ratios showed improved retention of the electrode thickness after 500 cycles. For example, the electrode with a Sn/C precursor ratio of 1.0 maintained ∼80% of the electrode thickness after 500 cycles, which might indicate that a thicker Nb−SnO_2 coating layer is more effective in providing protection from carbon corrosion. Nevertheless, we still cannot explain why a thicker coating layer of Nb−SnO_2 accelerates the performance degradation and increased polarization and resistance after 500 cycles.

Figure 6a,b presents SEM and EDS mapping results of cross-sectioned MEA cells before the stability test and after 500 cycles. The Nb−SnO_2-coated Pt/C electrodes are positioned on the lefthand side of the images. Before the stability test, Pt and Sn were, in general, uniformly distributed in the electrodes regardless of the Sn/C precursor ratios, whereas some Sn-rich agglomerates were found in the high Sn/C precursor ratio samples. Interestingly, more and larger Sn-rich agglomerates were formed after 500 cycles when the Sn/C precursor ratios increased (Figure 6b). Given the lower electronic conductivity of Nb−SnO_2 than carbon,[19] the agglomerated Nb−SnO_2 particles may block the electron pathways. We suspect that these agglomerated Nb−SnO_2 particles increase the tortuosity of the electron pathways and significantly increase the cell polarization.

4. DISCUSSION

Although Nb−SnO_2 coating layers improved ECSA retention, indicating that they can stabilize the electrode structure in principle, the formation of agglomerates after cycling suggests that further research is needed to optimize the coating uniformity and investigate the long-term stability of Nb−SnO_2 under PEMFC conditions. When the coating layer does not perfectly cover the carbon surfaces and has a nonuniform distribution on the carbon surfaces, the unprotected carbon surface degrades rapidly, creating agglomeration of coating materials. Therefore, the development of a uniform coating layer on the carbon surfaces is important to avoid any degradation of uncovered carbon surfaces. It is also possible that, due to the hydrophilic nature of SnO_2, the catalyst layer with agglomerated Nb−SnO_2 particles became more hydrophilic, and it would lead the water retention at local areas where Nb−SnO_2 agglomerates are. This behavior likely increases mass transport resistances at high current densities. Moreover, recent studies have shown that even materials previously assumed to be stable, such as TiO_2, can experience

https://doi.org/10.1021/acs.energyfuels.4c02232
Energy Fuels 2024, 38, 14655−14662

degradation in PEMFC environments,[30] emphasizing the importance of thorough stability investigations for novel coating materials like Nb−SnO_2.

5. CONCLUSIONS

In this study, we applied a protective layer coating of Nb-doped SnO_2 (Nb−SnO_2) nanoparticles on Pt/C catalysts at varied concentrations, spanning from 0.25:1 to 2.0:1 (Sn/C in a precursor ratio). When a higher concentration of Sn precursors was used, relatively large Nb−SnO_2 agglomerates formed and a heterogeneous distribution of Nb−SnO_2 nanoparticles was confirmed. Interestingly, contradictory behaviors of the Nb−SnO_2 coated Pt/C materials synthesized at different Sn/C ratios were observed. A higher Sn/C ratio sample exhibited improved ECSA retention after 500 cycles of AST but more significant polarization and resistance increase in the polarization curves after 500 cycles. Our post-mortem analysis demonstrated that Nb−SnO_2 particles became agglomerated when a higher Sn/C ratio sample was used in MEA testing although the shrinkage of the thickness of the Nb−SnO_2-coated Pt/C electrode was smaller than for a sample with a lower Sn/C ratio. We expect that the Nb−SnO_2 agglomerates form once the protective layer is broken down or the unprotected carbon surface is corroded, and the Nb−SnO_2 agglomerates increase the tortuosity of the electron pathways and significantly increase the cell polarization.

■ ASSOCIATED CONTENT

Supporting Information

The Supporting Information is available free of charge at https://pubs.acs.org/doi/10.1021/acs.energyfuels.4c02232.

TGA, SEM-EDS, and STEM-EDS data (PDF)

■ AUTHOR INFORMATION

Corresponding Authors

Lei Cheng − *Research and Technology Center, Robert Bosch LLC, Sunnyvale, California 94085, United States;* orcid.org/0000-0001-5498-9246; Email: Lei.Cheng2@us.bosch.com

Haegyeom Kim − *Materials Sciences Division, Lawrence Berkeley National Laboratory, Berkeley, California 94720, United States;* orcid.org/0000-0002-5962-8244; Email: haegyumkim@lbl.gov

Authors

Young-Woon Byeon − *Materials Sciences Division, Lawrence Berkeley National Laboratory, Berkeley, California 94720, United States;* orcid.org/0000-0003-2684-7720

Shirin Mehrazi − *Research and Technology Center, Robert Bosch LLC, Sunnyvale, California 94085, United States*

Björn M. Stühmeier − *Research and Technology Center, Robert Bosch LLC, Sunnyvale, California 94085, United States*

Venkata Sai Avvaru − *Materials Sciences Division, Lawrence Berkeley National Laboratory, Berkeley, California 94720, United States*

Dong-Min Kim − *Molecular Foundry Division, Lawrence Berkeley National Laboratory, Berkeley, California 94720, United States*

Brett A. Helms − *Materials Sciences Division, Lawrence Berkeley National Laboratory, Berkeley, California 94720, United States; Molecular Foundry Division, Lawrence Berkeley National Laboratory, Berkeley, California 94720, United States;* orcid.org/0000-0003-3925-4174

Complete contact information is available at: https://pubs.acs.org/10.1021/acs.energyfuels.4c02232

Author Contributions

‖Y. -W. B. and S. M. contributed to this work equally. Y. -W. B.: Investigation, data curation, visualization, and writing—original draft. S. M.: Investigation, data curation, visualization, and writing—original draft. B. M. S.: Investigation and data curation. V. S. A.: Investigation, and data curation. D. -M. K: Investigation and data curation. B. A. H.: Supervision. L. C.: Conceptualization, data curation, investigation, visualization, supervision, and writing—original draft. H. K.: Conceptualization, funding acquisition, data curation, investigation, visualization, supervision, and writing—original draft. All: Writing—review and editing.

Notes

The authors declare no competing financial interest.

■ ACKNOWLEDGMENTS

Work at the Molecular Foundry was supported by the Office of Science, Office of Basic Energy Sciences, of the U.S. Department of Energy under contract no. DE-AC02-05CH11231. We acknowledge Jeonghoon Lim for discussion of the material property measurements.

■ REFERENCES

(1) Parekh, A. Recent developments of proton exchange membranes for PEMFC: A review. *Front. Energy Res.* **2022**, *10*..

(2) Veeranjaneyulu, K.; Joshi, S.; Devalla, V.; Kiran, K. S. Khushal. Recent advancements of PEMFC in transport applications. *AIP Conf. Proc.* **2023**, *2492* (1), 050019.

(3) Alaswad, A.; Baroutaji, A.; Achour, H.; Carton, J.; Al Makky, A.; Olabi, A. G. Developments in fuel cell technologies in the transport sector. *Int. J. Hydrogen Energy* **2016**, *41* (37), 16499−16508.

(4) Wu, D.; Peng, C.; Yin, C.; Tang, H. Review of System Integration and Control of Proton Exchange Membrane Fuel Cells. *Electrochem. Energy Rev.* **2020**, *3* (3), 466−505.

(5) Barbir, F.; Gómez, T. Efficiency and economics of proton exchange membrane (PEM) fuel cells. *Int. J. Hydrogen Energy* **1997**, *22* (10−11), 1027−1037.

(6) Yu, X.; Ye, S. Recent advances in activity and durability enhancement of Pt/C catalytic cathode in PEMFC: Part II: Degradation mechanism and durability enhancement of carbon supported platinum catalyst. *J. Power Sources* **2007**, *172* (1), 145−154.

(7) Sim, J.; Kang, M.; Min, K.; Lee, E.; Jyoung, J.-Y. Effects of carbon corrosion on proton exchange membrane fuel cell performance using two durability evaluation methods. *Renewable Energy* **2022**, *190*, 959−970.

(8) Li, Y.; Zheng, Z.; Chen, X.; Liu, Y.; Liu, M.; Li, J.; Xiong, D.; Xu, J. Carbon corrosion behaviors and the mechanical properties of proton exchange membrane fuel cell cathode catalyst layer. *Int. J. Hydrogen Energy* **2020**, *45* (43), 23519−23525.

(9) Zhao, J.; Tu, Z.; Chan, S. H. Carbon corrosion mechanism and mitigation strategies in a proton exchange membrane fuel cell (PEMFC): A review. *J. Power Sources* **2021**, *488*, 229434.

(10) Chen, H.; Zhao, X.; Zhang, T.; Pei, P. The reactant starvation of the proton exchange membrane fuel cells for vehicular applications: A review. *Energy Convers. Manage.* **2019**, *182*, 282−298.

(11) Yousfi-Steiner, N.; Moçotéguy, P.; Candusso, D.; Hissel, D. A review on polymer electrolyte membrane fuel cell catalyst degradation and starvation issues: Causes, consequences and diagnostic for mitigation. *J. Power Sources* **2009**, *194* (1), 130−145.

(12) Wu, H.; Wexler, D.; Liu, H. Durability investigation of graphene-supported Pt nanocatalysts for PEM fuel cells. *J. Solid State Electrochem.* **2011**, *15* (5), 1057−1062.
(13) Xue, Q.; Huang, J.-b.; Yang, D.-j.; Li, B.; Zhang, C.-m. Enhanced PEMFC durability with graphitized carbon black cathode catalyst supports under accelerated stress testing. *RSC Adv.* **2021**, *11* (32), 19417−19425.
(14) Qiao, Z.; Hwang, S.; Li, X.; Wang, C.; Samarakoon, W.; Karakalos, S.; Li, D.; Chen, M.; He, Y.; Wang, M.; et al. 3D porous graphitic nanocarbon for enhancing the performance and durability of Pt catalysts: a balance between graphitization and hierarchical porosity. *Energy Environ. Sci.* **2019**, *12* (9), 2830−2841.
(15) Wei, L.; Shi, J.; Cheng, G.; Lu, L.; Xu, H.; Li, Y. Pt/TiN−TiO2 catalyst preparation and its performance in oxygen reduction reaction. *J. Power Sources* **2020**, *454*, 227934.
(16) Byeon, Y.-W.; Mailoa, J.; Kornbluth, M.; Lee, G.-H.; Cai, Z.; Sun, Y.; Yang, W.; Johnston, C.; Christensen, J.; Kim, S.; et al. Electronic structure manipulation via composition tuning for the development of highly conductive and acid-stable oxides. *J. Mater. Chem. A* **2022**, *10* (43), 23155−23164.
(17) Lee, E.; Park, C.; Lee, D. W.; Lee, G.; Park, H.-Y.; Jang, J. H.; Kim, H.-J.; Sung, Y.-E.; Tak, Y.; Yoo, S. J. Tunable Synthesis of N,C-Codoped Ti3+-Enriched Titanium Oxide Support for Highly Durable PEMFC Cathode. *ACS Catal.* **2020**, *10* (20), 12080−12090.
(18) Naik, K. M.; Higuchi, E.; Inoue, H. Two-dimensional oxygen-deficient TiO2 nanosheets-supported Pt nanoparticles as durable catalyst for oxygen reduction reaction in proton exchange membrane fuel cells. *J. Power Sources* **2020**, *455*, 227972.
(19) Takasaki, F.; Matsuie, S.; Takabatake, Y.; Noda, Z.; Hayashi, A.; Shiratori, Y.; Ito, K.; Sasaki, K. Carbon-Free Pt Electrocatalysts Supported on SnO2 for Polymer Electrolyte Fuel Cells: Electrocatalytic Activity and Durability. *J. Electrochem. Soc.* **2011**, *158* (10), B1270.
(20) Senoo, Y.; Kakinuma, K.; Uchida, M.; Uchida, H.; Deki, S.; Watanabe, M. Improvements in electrical and electrochemical properties of Nb-doped SnO2−δ supports for fuel cell cathodes due to aggregation and Pt loading. *RSC Adv.* **2014**, *4* (61), 32180−32188.
(21) Dubau, L.; Maillard, F.; Chatenet, M.; Cavaliere, S.; Jiménez-Morales, I.; Mosdale, A.; Mosdale, R. Durability of Alternative Metal Oxide Supports for Application at a Proton-Exchange Membrane Fuel Cell Cathode—Comparison of Antimony- and Niobium-Doped Tin Oxide. *Energies* **2020**, *13* (2), 403.
(22) Inaba, M.; Murase, R.; Takeshita, T.; Yano, K.; Kosaka, S.; Takahashi, N.; Isomura, N.; Oh-ishi, K.; Yoshimune, W.; Tsuchiya, K.; et al. Synthesis of a Mesoporous SnO2 Catalyst Support and the Effect of Its Pore Size on the Performance of Polymer Electrolyte Fuel Cells. *ACS Appl. Mater. Interface* **2024**, *16* (8), 10295−10306.
(23) Fukuda, T.; Iimura, K.; Yamamoto, T.; Tsuji, R.; Tanabe, M.; Nakashima, S.; Fukumuro, N.; Ito, S. Ozone-Assisted Hydrothermal Synthesis Method of Sb-Doped SnO2 Conductive Nanoparticles for Carbon-Free Oxygen-Reduction-Reaction Catalysts of Proton-Exchange-Membrane Hydrogen Fuel Cells. *Crystals* **2024**, *14* (5), 462.
(24) Cao, W.; Mao, Y.; Hu, B.; Yang, Y.; Zhou, W.; Shao, Z. Significantly improved stability and water retention for Pt supported on W-doped SnO2 to catalyse the oxygen reduction reaction in proton exchange membrane fuel cells. *J. Mater. Chem. A* **2024**, *12* (18), 10799−10807.
(25) Dou, M.; Hou, M.; Liang, D.; Lu, W.; Shao, Z.; Yi, B. SnO2 nanocluster supported Pt catalyst with high stability for proton exchange membrane fuel cells. *Electrochim. Acta* **2013**, *92*, 468−473.
(26) Min, H.; Choi, J.-H.; Kang, H. E.; Kim, D.-J.; Yoon, Y. S. Enhanced Durability and Catalytic Performance of Pt−SnO2/Multi-Walled Carbon Nanotube with Shifted d-Band Center for Proton-Exchange Membrane Fuel Cells. *Small Structures* **2024**, *5* (3), 2300407.
(27) Macauley, N.; Papadias, D. D.; Fairweather, J.; Spernjak, D.; Langlois, D.; Ahluwalia, R.; More, K. L.; Mukundan, R.; Borup, R. L. Carbon Corrosion in PEM Fuel Cells and the Development of Accelerated Stress Tests. *J. Electrochem. Soc.* **2018**, *165* (6), F3148−F3160.
(28) Saha, P.; Khedekar, K.; Wang, H.; Atanassov, P.; Cheng, L.; Stewart, S.; Johnston, C.; Zenyuk, I. V. Correlating the morphological changes to electrochemical performance during carbon corrosion in polymer electrolyte fuel cells. *J. Mater. Chem. A* **2022**, *10* (23), 12551−12562.
(29) Bandlamudi, V.; Bujlo, P.; Sita, C.; Pasupathi, S. Study on electrode carbon corrosion of high temperature proton exchange membrane fuel cell. *Mater. Today: Proc.* **2018**, *5*, 10602−10610.
(30) Zhang, J.; Coms, F. D.; Kumaraguru, S. Necessity to Avoid Titanium Oxide As Catalyst Support in PEM Fuel Cells. *ECS Meeting Abstracts* **2019**, *MA2019-01* (30), 1481.

https://doi.org/10.1021/acs.energyfuels.4c02232
Energy Fuels 2024, 38, 14655−14662